Mercury(II) Ion Adsorption Behavior in Thiol-Functionalized Mesoporous Silica Microspheres

Ashley Bibby and Louis Mercier*

Department of Chemistry and Biochemistry, Laurentian University, Sudbury, Ontario, Canada P3E 2C6

Received August 7, 2001. Revised Manuscript Received November 26, 2001

Microspherical mercury ion adsorbents with uniform mesopore channels were prepared by fluoride-catalyzed surfactant-directed co-condensation of tetraethoxysilane (TEOS) and 3-mercaptopropyltrimethoxysilane (MPTMS) using mildly acidic nonionic surfactant solutions. Using batch adsorption methods, mercury(II) adsorption isotherms and kinetic uptake profiles for these adsorbents were obtained. The mercury(II) isotherms of the microspheres with low thiol group loadings did not fit the Langmuir expression and were indicative of weak interactions between the mercury(II) ions and the adsorbents. With increasing thiol group loading, the isotherms approached type-I in appearance, indicating improved binding energetics of the ions with the adsorbents. The adsorption kinetics of the adsorbents suggested that the uptake of mercury ions by the microspheres was rather slow, with diffusion coefficients ranging between 10^{-14} and 10^{-15} m^2 s^{-1}. The coefficients were found to increase as a function of the thiol group density of the adsorbents. The diffusion coefficients of the mercury(II) adsorption process were also found to increase as a function of time, indicating synergistic acceleration of the uptake rate with increasing mercury ion loading in the materials. On the basis of these observed trends, an ion permeation and displacement mechanism is proposed and described.

Introduction

The discovery that silica and other metal oxides with uniform mesoscale pore channels could be prepared by surfactant-mediated assembly has, during the past 10 years, intensified research interests in the synthesis and inclusion chemistry of nanoporous materials.[1−33] Unlike typical sol−gel-derived oxides, which are crystallographically amorphous and have ill-defined pore channel structures, surfactant-assembled mesoporous oxides (also denoted mesoporous molecular sieves or mesostructures) exhibit long-range order and have uniform-diameter pore channels (typically in the range 2−10 nm). That the surface areas of mesoporous molecular sieves can be as high as 1500 m^2 g^{-1} makes these materials especially interesting from a surface science point of view. Various surfactant assembly methods have been developed to form a wide range of nanoporous oxides with different pore structures, particle shapes,

* To whom correspondence should be addressed.

(1) Kresge, C. T.; Leonowicz, M. E.; Roth, W. J.; Vartuli, J. C.; Beck, J. S. *Nature* **1992**, *359*, 710.
(2) Beck, J. S.; Vartuli, J. C.; Roth, W. J.; Leonowicz, M. E.; Kresge, C. T.; Schmitt, K. D.; Chu, C. T.-W.; Olson, D. H.; Sheppard, E. W.; McCullen, S. B.; Higgins, J. B.; Schlenker, J. L. *J. Am. Chem. Soc.* **1992**, *114*, 10834.
(3) Monnier, A.; Schuth, F.; Huo, Q.; Kumar, D.; Margolese, D.; Maxwell, R. S.; Stucky, G. D.; Krishnamurty, M.; Petroff, P.; Firouzi, A.; Janicke, M.; Chmelka, B. F. *Science* **1993**, *261*, 1299.
(4) Huo, Q.; Margolese, D. I.; Ciesla, U.; Feng, P.; Gier, T. E.; Sieger, P.; Leon, R.; Petroff, P. M.; Schuth, F.; Stucky, G. D. *Nature* **1994**, *368*, 317.
(5) Huo, Q.; Margolese, D. I.; Ciesla, U.; Demuth, D. G.; Feng, P.; Gier, T. E.; Sieger, P.; Forouzi, A.; Chmelka, B. F.; Schuth, F.; Stucky, G. D. *Chem. Mater.* **1994**, *6*, 1176.
(6) Mann, S.; Ozin, G. A. *Nature* **1996**, *376*, 313.
(7) Yang, H.; Coombs, N.; Ozin, G. A. *Nature* **1997**, *386*, 692.
(8) Yang, H.; Ozin, G. A.; Kresge, C. T. *Adv. Mater.* **1998**, *10*, 883.
(9) Yang, S. M.; Yang, H.; Coombs, N.; Sokolov, I.; Kresge, C. T.; Ozin, G. A. *Adv. Mater.* **1999**, *11*, 52.
(10) Tanev, P. T.; Pinnavaia, T. J. *Science* **1995**, *267*, 865.
(11) Tanev, P. T.; Pinnavaia, T. J. *Chem. Mater.* **1996**, *8*, 2068.
(12) Zhang, W.; Pauly, T. R.; Pinnavaia, T. J. *Chem. Mater.* **1997**, *9*, 2491.
(13) Bagshaw, S. A.; Prouzet, E.; Pinnavaia, T. J. *Science* **1995**, *269*, 1242.
(14) Prouzet, E.; Pinnavaia, T. J. *Angew. Chem., Int. Ed. Engl.* **1997**, *36*, 516.
(15) Prouzet, E.; Cot, F.; Nabias, G.; Larbot, A.; Kooyman, P.; Pinnavaia, T. J. *Chem. Mater.* **1999**, *11*, 1498.
(16) Boissière, C.; van der Lee, A.; El Mansouri, A.; Larbot, A.; Prouzet, E. *Chem Commun.* **1999**, 2047.
(17) Boissière, C.; Larbot, A.; van der Lee, A.; Kooyman, P. J.; Prouzet, E. *Chem. Mater.* **2000**, *12*, 2902.
(18) Boissière, C.; Larbot, A.; Prouzet, E. *Chem. Mater.* **2000**, *12*, 1937.
(19) Antonelli, D. M.; Ying, J. Y. *Angew. Chem., Int. Ed. Engl.* **1996**, *35*, 426.
(20) Antonelli, D. M.; Ying, J. Y. *Chem. Mater.* **1996**, *8*, 874.
(21) Moller, K.; Bein, T. *Chem. Mater.* **1998**, *10*, 2950.
(22) Mercier, L.; Pinnavaia, T. J. *Chem. Mater.* **2000**, *12*, 188.
(23) Richer, R.; Mercier, L. *J. Chem. Soc., Chem. Commun.* **1998**, 1775.
(24) Richer, R.; Mercier, L. *Chem. Mater.* **2001**, *13*, 2999.
(25) Mercier, L.; Pinnavaia, T. J. *Adv. Mater.* **1997**, *9*, 500.
(26) Feng, X.; Fryxell, G. E.; Wang, L.-Q.; Kim, A. Y.; Liu, J.; Kemner, K. M. *Science* **1997**, *276*, 923.
(27) L. Mercier; Pinnavaia, T. J. *Microporous Mesoporous Mater.* **1998**, *20*, 101.
(28) Lim, M. H.; Blanford, C. F.; Stein, A. *Chem. Mater.* **1998**, *10*, 467.
(29) Mercier, L.; Pinnavaia, T. J. *Environ. Sci. Technol.* **1998**, *32*, 2749.
(30) Brown, J.; Mercier, L.; Pinnavaia, T. J. *J. Chem. Soc., Chem. Commun.* **1999**, 69.
(31) Brown, J.; Richer, R.; Mercier, L. *Microporous Mesoporous Mater.* **2000**, *37*, 41.
(32) Mercier, L. *Stud. Surf. Sci. Catal.* **2000**, *129*, 739.
(33) Pauly, T. R.; Liu, Y.; Pinnavaia, T. J.; Billinge, S. J. L.; Rieker, T. P. *J. Am. Chem. Soc.* **1999**, *121*, 8835.

10.1021/cm0112082 CCC: $22.00
Published on Web 03/12/2002

and textures, properties that are determined by the nature of interactions between the surfactant and the inorganic precursors used in the parent synthesis mixtures.[1−20]

The earliest attempts at forming mesostructured oxides involved the use of electrostatic (ionic) surfactant−precursor assembly interactions and succeeded in forming materials with crystallographically well-ordered pore channels and monolithic micrometric particles.[1−9] These mesostructures have been designated as the M41S class of materials[1,2] (including the hexagonal MCM-41 and the cubic MCM-48 structure types) and the SBA class of materials.[3−5] Subsequently, other surfactant−precursor assembly interactions leading to mesostructure formation have been identified, including hydrogen bonding (forming the HMS[10,11] and MSU-X[13−18] classes of materials) and coordinative attachment.[19,20] The HMS and MSU-X classes of mesostructures can be distinguished from the M41S and SBA materials by their wormhole-motif pore channel structures, which are devoid of any space symmetry.[10−18] Moreover, these materials typically have very small (submicron) fundamental particle sizes with which is often associated a high degree of textural (interparticle) porosity.[10−15,25]

The development of functionalized nanoporous materials for adsorption applications has generated much research attention.[21−32] In particular, the preparation of highly effective adsorbents for heavy metal ion trapping by the grafting or incorporation of ligands into mesostructured oxides has been identified as a most promising avenue for environmental cleanup applications.[25−32] An important advantage that was identified for these types of adsorbents is their comparatively large (nanometer-scale) open-framework pore structure, which, unlike the structures of materials with disordered and microporous pore channels (e.g., silica gel and clays), allow uninhibited access of the metal ions to every ligand site in the structure.[25,26,29,31] This advantage has allowed for the preparation of mercury ion adsorbents with unprecedentedly high binding capacity, as pore constriction does not occur in these materials.

So far, the influence of mesostructure particle morphology on the adsorption properties of mesostructured adsorbents has not been investigated in great detail. This is likely because most mesostructure synthesis protocols produce materials with ill-defined particle shapes and broad particle size distributions, thus hindering accurate studies concerning mesostructure morphology. Although synthesis methods producing mesostructures with well-defined particle shapes have been reported,[6−9] these structures often have exotic morphologies and pore channel openings located only on restricted regions on the particles. These materials would therefore not be suitable for the study of morphological influences on bulk adsorption properties as any interpretation of results would be very difficult given the complex nature of these particle shapes. Recently, however, the synthesis of mesoporous MSU-X silica with a spherical particle morphology and narrow size distribution (6−12 μm in diameter) was described.[16,17] As is common for any wormhole-motif MSU-X mesostructure, these materials have pore channel openings throughout the outer surface of their particles, and the pore channels twist and turn randomly within the mesostructure particles.[13−18,33] The spherical shape, particle size uniformity, and randomness of pore channel directionality make these microspherical MSU-X silicas ideal for studying host−guest interactions that occur within the pore channels of mesostructured adsorbents with well-defined particle morphologies. In the current study, the thermodynamic and kinetic behavior of mercury ion adsorption within the pore channels of thiol-functionalized microspherical mesoporous silica is investigated.

Experimental Section

Chemicals. All compounds used in this work were supplied by Aldrich Chemicals, Mississauga, Ontario, Canada.

Adsorbents. *Thiol-Functionalized Mesoporous Silica Microspheres*. The microspherical mesoporous adsorbents were prepared using a one-step functionalization method[22,23] adapted to the microspherical MSU-X synthesis procedure described by Boissière et al.[16,17] Thus, $(1 - X) \times 2.16 \times 10^{-2}$ mol of tetraethoxysilane (TEOS) and $X \times 2.16 \times 10^{-2}$ mol of 3-mercaptopropyltrimethoxysilane (MPTMS, $X = 0$, 0.02, 0.04 or 0.06) were mixed then added to 100 mL of aqueous Triton-X-100 solution (0.027 mol L^{-1}). Five milliliters of 0.20 mol L^{-1} HCl was then added and the mixture was stirred until it became completely clear. Then, 8.8 mg of NaF was added, and after a few seconds of stirring, agitation was stopped, and the solutions were allowed to sit undisturbed for 24 h to allow product formation. The resulting material was then filtered, washed by Soxhlet extraction over ethanol for 48 h, and air-dried. The mesostructures thus obtained are hereafter denoted MP-MSU-0%, MP-MSU-2%, MP-MSU-4%, and MP-MSU-6% (the percentage refers to the relative amount of silane used in the synthesis in the form of MPTMS, or 100X).

Characterization of Microspherical MP-MSU Mesostructures. Powder X-ray diffraction patterns were measured on a Rigaku Rotaflex diffractometer equipped with a rotating anode using Cu Kα radiation (Ontario Geosciences Laboratories, Sudbury, Ontario, Canada).

N_2 adsorption−desorption isotherms of the adsorbents were measured at −196 °C on a Micromeritics ASAP 2010 sorptometer. Prior to measurement, all samples were outgassed at 110 °C and 10^{-6} mmHg. BET surface areas were measured from the linear part of the BET plot ($0.05 < P/P^0 < 0.25$).[34,35] Pore size distributions were calculated from the adsorption branch of the isotherms using the Broekhoff−deBoer model.[36]

SEM images of the adsorbents were obtained using a JEOL JSM6400 scanning electron microscope (Ontario Geosciences Laboratories).

Particle size distributions of the adsorbents were measured using a Microtrac laser diffraction particle size analyzer (Ontario Geosciences Laboratories).

Mercury Ion Adsorption Isotherms. The Hg^{2+} adsorption isotherms for each MP-MSU mesostructure were measured using a batch adsorption process. Thus, a 5-mg sample of adsorbent was slurried in 25 mL of distilled water. Twenty-five milliliters of $Hg(NO_3)_2$ stock solution (25 ppm in Hg^{2+}) was added to the slurry, and the mixture was stirred for 24 h, by which time it was assumed that adsorption equilibrium had been reached. The treated solution was then filtered, and the mercury(II) ion concentration remaining in the solution was measured by cold-vapor AAS (Laurentian University Central Analytical Facility, Sudbury, Ontario, Canada). This process was repeated using $Hg(NO_3)_2$ solutions with varying concentrations (up to 150 ppm in Hg^{2+}).

Mercury Ion Diffusion Kinetics. A stock solutions of $Hg(NO_3)_2$ (140 ppm in Hg^{2+}) was prepared for the kinetic

(34) Brunnauer, S.; Emmet, P. H.; Teller, E. *J. Am. Chem. Soc.* **1938**, *60*, 309.
(35) Brunnauer, S.; Deming, L. S.; Deming, W. S.; Teller, E. *J. Am. Chem. Soc.* **1940**, *62*, 1723.
(36) Broekhoff, J. C. P.; de Boer, J. H. *J. Catal.* **1968**, *10*, 377.

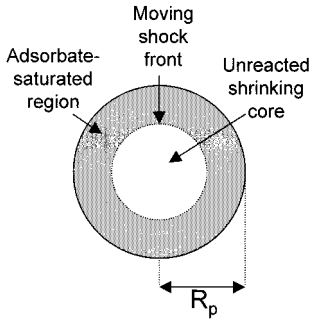

Figure 1. Shrinking core model representation of adsorbate diffusion within a spherical adsorbent particle of radius R_p.[38]

experiments and assayed by cold-vapor AAS [the initial mercury ion concentration used for the uptake experiments (140 ppm) was selected to be sufficiently high to ensure that the residual mercury concentration never reached levels that were below that required to fulfill thermodynamic equilibrium conditions for each adsorbent]. For each MP-MSU adsorbent, 5-mg portions of material were slurried in 25 mL of distilled water. To each slurry, 25 mL of the Hg(II) stock solution was added, and the suspension was stirred for time periods ranging from 30 to 600 s. The adsorption process was then stopped by rapidly filtering the suspension by suction through a Whatmann paper filter, ensuring that no adsorbent particles permeated through the filter. The residual mercury ion concentrations (C_t) remaining in the filtrate solutions were then analyzed by cold-vapor AAS. The amount of mercury adsorbed at equilibrium (C_∞) was likewise measured by allowing a sample of the adsorbent to stir for 24 h before filtering. The fraction of mercury ions remaining in solution, denoted χ, was then calculated using the formula $\chi = (C_t - C_\infty)/(C_i - C_\infty)$, where C_t is the mercury ion concentration remaining in solution after an exposure time t, C_∞ is the mercury ion concentration remaining in solution when equilibrium is achieved (viz., after an exposure time of 24 h), and C_i is the initial concentration of mercury ion (i.e., one-half the concentration of the stock solution). The mercury ion kinetic uptake profiles thus obtained were repeated in triplicate for each adsorbent.

Modeling of Uptake Kinetics. Mercury ion diffusion coefficients, D_p, for the adsorbents were calculated from their respective kinetic uptake data using the shrinking core model (SCM).[37] The model assumes penetration of the adsorbate species (Hg^{2+} ion) through a spherical adsorbent particle such that a moving "shock front" is produced, separating the adsorbate-saturated peripheral region of the particle from the shrinking core region in which the adsorbate has not yet penetrated (Figure 1). The SCM is thus only applicable to systems in which the adsorbent−adsorbate interactions are very strong and essentially irreversible, as in chemisorption. Because the binding of mercury ions with the thiol groups located inside mesostructure pore channels is very strong,[25,29−31] the SCM can be deemed appropriate for the determination of kinetic parameters for these systems. Moreover, that the MSU mesostructures used in this study consist of monodisperse microspheres make the usage of the SCM particularly suitable for the kinetic analysis of these systems. The relationship between the adsorbent exposure time (t) and fraction of mercury ions remaining in the treated solution (χ) can thus be represented by the expression[37]

$$6\epsilon_p D_p R_p^{-2} c_0 q_s^{-1} t = 1 + 2\chi - 3\chi^{2/3} \qquad (1)$$

where ϵ_p is the porosity fraction of the adsorbents, D_p is the pore diffusivity coefficient ($m^2\ s^{-1}$), R_p is the radius of the adsorbent particle (m), c_0 is the initial amount of Hg^{2+} in the solution (mg), and q_s is the saturation limit of Hg^{2+} in the adsorbent (mg). For each adsorbent, the porosity fraction ϵ_p was determined by dividing the total pore volume of the adsorbent (i.e., the maximum N_2 volume adsorbed by the material) by the material's skeletal volume (i.e., the combined volumes of both the pores and the framework of the material). For this purpose, it was assumed that the density of the bulk silica that constitutes the framework walls of the adsorbents was 2.2 g cm^{-3};[15] thus, the volume occupied by the framework in 1 g of silica corresponds to 0.45 cm^2. (Note that, because the thiol group contents of the adsorbents were negligible compared to the amount of SiO_2, all materials were essentially considered as being composed of pure silica for the purpose of this calculation. Also, the silica density of MSU-X walls is not actually known but has been referenced to that of dense bulk silica for the purposes of this work.) The porosity fraction, ϵ_p, of the adsorbents was thus calculated using the expression

$$\epsilon_p = V_p/(V_p + 0.45) \qquad (2)$$

where V_p is the liquid pore volume of the adsorbent expressed in $cm^3\ g^{-1}$.

(37) Ruthven, D. M., Kärger, J. *Diffusion in Zeolites*; Wiley-Interscience: New York, 1992; pp 250−255.

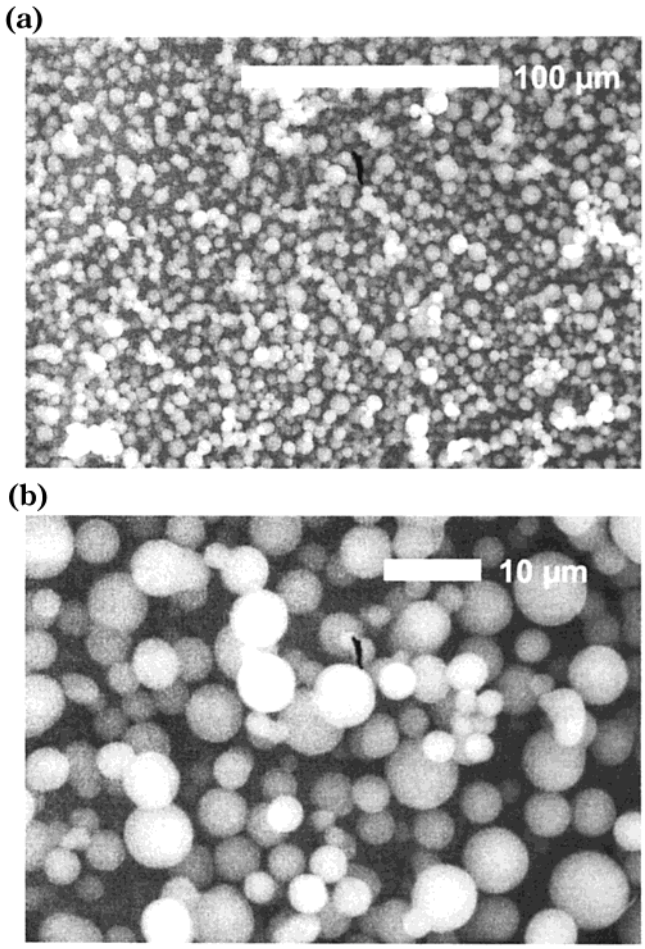

Figure 2. (a) Lower-resolution and (b) higher-resolution scanning electron micrographs of MP-MSU-4% microspheres.

Results and Discussion

Morphological and Structural Characterization of Adsorbents. Consistent with the results reported by Boissière et al.,[16] the SEM images of the adsorbents revealed that the MP-MSU mesostructures were spherical and monodisperse (Figure 2). Particle size analysis on the samples (Figure 3) confirmed the very narrow size distribution of the adsorbents, centered at mean diameters of 10−12 μm (Table 1).

Table 1. Physicochemical Characteristics of MP-MSU Microspheres

material	*d* spacing (Å)	BET surface area (m^2/g)	pore diameter, D_p (Å)	mean particle diameter, $2R_p$ (μm)	pore volume, V_p (cm^3g^{-1})	fractional porosity, ϵ_p	Hg^{2+} adsorption capacity (mmol/g)
MP-MSU-0%	42	1263	32	12.5	0.77	0.63	0
MP-MSU-2%	42	1175	29	10.7	0.62	0.58	0.52
MP-MSU-4%	40	1149	27	12.0	0.58	0.56	1.01
MP-MSU-6%	39	995	24	12.3	0.48	0.52	1.49

The XRD patterns of the microspheres (Figure 4) were typical of those obtained for wormhole-motif mesostructures,[13−18] featuring broad correlation peaks corresponding to average lattice spacings of 39−42 Å (Table 1). The observed reduction in peak intensity with increasing mercaptopropyl group loading within the mesostructures (Figure 4) can be ascribed to contrast matching between the incorporated sulfur atoms and the silica framework,[25,29] although structural perturbations resulting from the addition of organosilane in the synthesis mixture cannot be ruled out as another explanation for this observation.[23,24] A systematic shift of the peaks to higher diffraction angles, moreover, suggests that slight lattice contractions occur as a result of the incorporation of the organosilane groups within the mesostructure synthesis.[23,24] All of the aforementioned trends are in accord with those previously described for functionalized mesostructures prepared using the one-step synthesis methodology.[23,24]

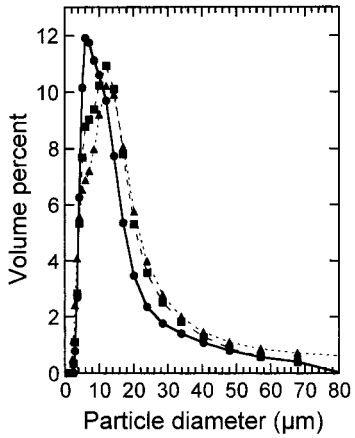

Figure 3. Particle size distributions of (- - -) MP-MSU-0%, (●) MP-MSU-2%, (■) MP-MSU-4%, and (▲) MP-MSU-6% microspheres.

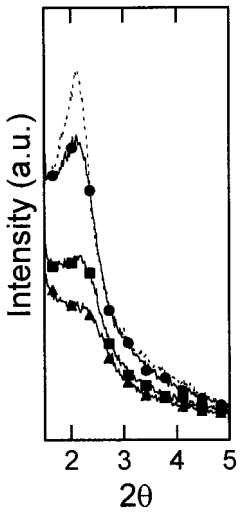

Figure 4. Powder X-ray diffraction patterns of (- - -) MP-MSU-0%, (●) MP-MSU-2%, (■) MP-MSU-4%, and (▲) MP-MSU-6% microspheres.

In addition, the N_2 isotherms of the materials (Figure 5) were typical of those reported for other mesostructured oxides,[1−33] featuring inflections in the range $0.15 < P/P^0 < 0.35$, indicating uniform framework mesoporosity. Using the isotherm data, the adsorbents were found to have very high pore volumes and surface areas (Table 1), as well as uniform pore channels in the range 24−32 Å. Moreover, the isotherms did not feature any hysteresis, and no upswing in the isotherm curve was observed as P/P^0 approached 1, indicating that the microspheres were devoid of any textural porosity. Hence, the adsorbent microspheres consisted entirely of single-domain mesoporous silica whose porosity was entirely and exclusively generated by the surfactant assembly process (viz., the porosity of the particles arises only from the mesopore channels therein and not from textural features such as cracks and voids). These microspheres are therefore very useful for the study of inclusion phenomena occurring exclusively within the mesopore channels of the surfactant-assembled adsorbents.

The pore volumes, pore diameters, surface areas, and porosity fractions of the MP-MSU materials were all found to decrease as a function of increasing MP group loading inside the materials (Table 1). The increasing loading of the pore channels with the functional groups thus results in increasing congestion of the pore channels with the mercaptopropyl groups, giving rise to the observed trends in surface properties.[22−25] All of the mesostructures nonetheless retained adequate porosity to act as potentially effective mercury ion adsorbents.

Mercury Ion Adsorption Isotherms. The Hg(II) adsorption isotherms of the MP-MSU adsorbents (Figure 6) showed that the mercury ions adsorbed until saturation was reached at levels depending on the MP group loading level in the adsorbent (Table 1). It has been widely documented that thiol-functionalized me-

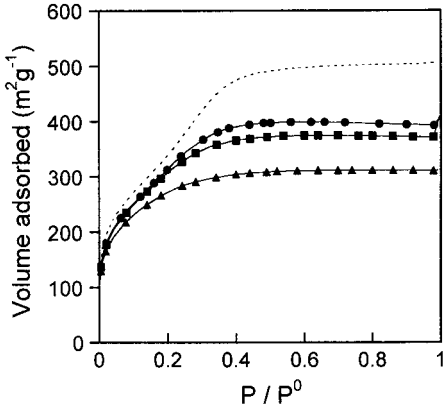

Figure 5. N_2 adsorption isotherms of (- - -) MP-MSU-0%, (●) MP-MSU-2%, (■) MP-MSU-4%, and (▲) MP-MSU-6% microspheres.

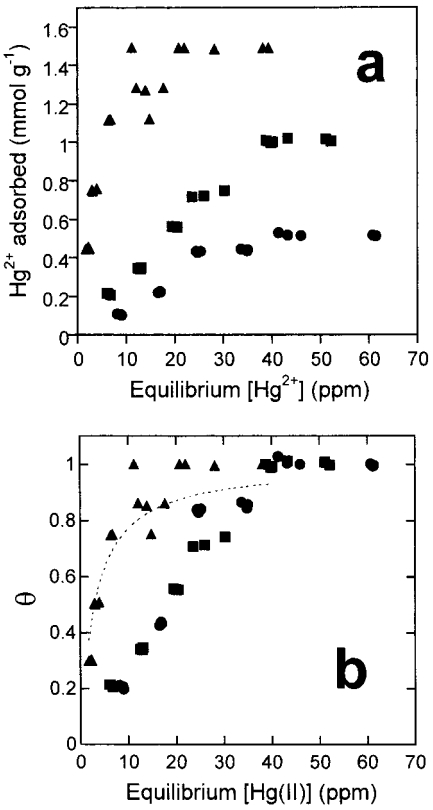

Figure 6. Hg^{2+} adsorption isotherms for (●) MP-MSU-2%, (■) MP-MSU-4%, and (▲) MP-MSU-6% microspherical adsorbents expressed (a) in terms of the amount of adsorbed ions and (b) in terms of the binding site (viz., thiol group) fractional coverage θ. The dashed line in b is the fit of the MP-MSU-6% isotherm data to the Langmuir equation.

sostructured adsorbents with pore diameters larger than 2 nm bind mercury ions with every thiol group present in the materials.[25−32] It can thus be surmised that the thiol group loadings in the MP-MSU microspheres should be equivalent to their respective mercury ion binding capacities (Table 1).

The Hg^{2+} adsorption isotherms for MP-MSU-2% and MP-MSU-4% were type-V in appearance[38] (Figure 6b), featuring nonquantitative adsorptivity at low ion concentrations (viz., significant residual mercury ion levels remained in solution). Hence, attempts at fitting the isotherm data for these adsorbents with the Langmuir expression[39] [i.e., $\theta = b[Hg^{2+}]/(1 + b[Hg^{2+}])$, where θ represents the fractional coverage of binding (thiol) sites and b represents an equilibrium constant for the adsorption process] did not give statistically significant fits, as this model is applicable only in the case of type-I isotherms. The type-V appearance of these isotherms plausibly indicates a lack of energetic uniformity of the thiol groups within the mesostructures for mercury ion binding. The mercury ion adsorption profiles suggest that, at low mercury ion concentrations, the binding energy of the ions is somewhat low and, thus, relatively few thiol sites are accessed by the mercury ions. Only when the mercury ion concentrations become sufficiently high (about 40 ppm under the experimental conditions used in this study) can the ions be driven to bind with every thiol group in the adsorbents. In contrast to the results obtained in this work, previous studies on mercury ion adsorption using thiol-functionalized HMS and MSU mesostructures reported good fits to the Langmuir expression.[25,29−31] These materials, however, were characterized as having very high degrees of textural porosity and/or very small fundamental particle sizes (<0.3 μm in diameter), features that readily provide access to the thiol groups in the mesostructures. The availability of the thiol groups for binding with the ions thus effectively improves the binding energetics of the ligands within the nanoscopic particles of these mesostructures. Mesostructures with larger particle sizes and no textural porosity, however, demonstrate difficulty in providing similar access of the binding sites to the solution-phase ions (this being especially true for the sites located deep within the particles). Isotherms similar to those observed in Figure 6 have also been observed for thiol-functionalized MCM-41,[29] which also had large particle sizes and little textural porosity.

In contrast to the mercury ion adsorption isotherms of MP-MSU-2% and MP-MSU-4%, that of MP-MSU-6% had a much steeper adsorption profile for mercury ions (Figure 6b), approaching the ideal type-I isotherm shape. This isotherm had a better fit to the Langmuir expression than those of the other more sparsely functionalized microspheres, although the fit was not significant enough ($R^2 = 0.86$) to allow for a suitable determination of thermodynamic parameters. The increased steepness of the Hg^{2+} isotherm for MP-MSU-6% can be attributed to the increased thiol group density in this material, which facilitates the ability of the material to adsorb the metal ions, especially at low concentration.

The physical characteristics (d spacing, pore diameter) and thiol group content of MP-MSU-6% (1.49 mmol/g) were similar to those reported for MP−HMS prepared by the grafting process.[25] It can thus be inferred that the spacing between thiol groups within MP-MSU-6% should be similar to that estimated for MP−HMS (about 20 Å between groups).[25] Given the relative proximity of the ligand sites at this surface group density, it can be postulated that the enhanced Hg^{2+} binding affinity of MP-MSU-6% compared to those of MP-MSU-2% and MP-MSU-4% results from the presence of thermodynamically more active binding sites (such as those resulting from bidentate complexation, for instance). This situation would facilitate the adsorption of mercury ions from solution at low solute concentrations.

Mercury Ion Adsorption Kinetics. Figure 7 displays the mercury ion uptake curves for the three microspherical adsorbents. The uptake data, which were measured in triplicate, displayed remarkable reproducibility, as evidenced by the generally small standard deviations (error bars) in the values (Figure 7).

One of the expected advantages of materials with uniform mesoscale porosities is their expected improved rate of guest−host reactivity (viz., adsorption or catalysis) compared to materials with ill-defined porosity or microporous size ranges. However, despite the high surface areas and uniform mesoporosities of the microspherical adsorbents, the results shown in Figure 7 do

(38) Brunauer, S. *The Adsorption of Gases and Vapors*; Princeton University Press: Princeton, NJ, 1945; Vol. 1.
(39) Langmuir, I. *J. Am. Chem. Soc.* **1918**, *40*, 1361.

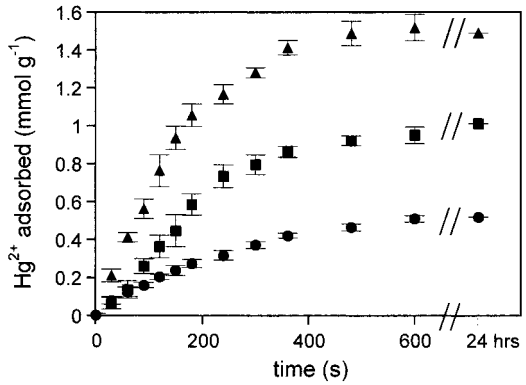

Figure 7. Hg^{2+} kinetic uptake curves for (●) MP-MSU-2%, (■) MP-MSU-4%, and (▲) MP-MSU-6% microspherical adsorbents. The error bars represent the standard deviations obtained from triplicate experiments at each exposure time.

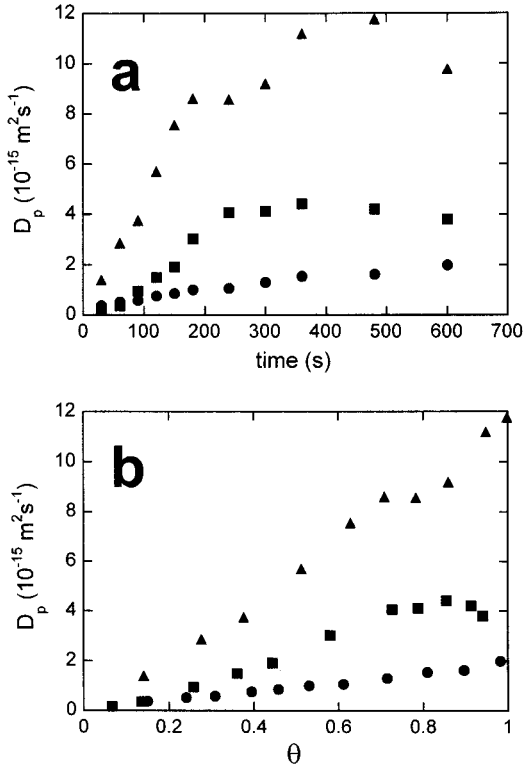

Figure 8. Hg^{2+} diffusion coefficients, D_p, for (●) MP-MSU-2%, (■) MP-MSU-4%, and (▲) MP-MSU-6% microspherical adsorbents expressed (a) as a function of exposure time and (b) as a function of binding site (viz., thiol group) coverage.

not demonstrate any remarkably rapid mercury ion uptake by the mesostructures. In fact, the adsorption process of the materials appears to be rather sluggish, with access to 50% of the binding sites requiring approximately between 100 and 200 s of contact time with the mercury ion solutions, and total access to the sites requiring more than 500 s of contact time (Figure 7).

The diffusion coefficients (D_p) calculated for the adsorbents using the uptake data (Figure 8) also concur with the slow diffusion of mercury ions inside the mesoporous adsorbents that was evident upon cursory inspection of the uptake curve. In all cases, the maximum D_p values for the adsorbents were generally in the range 10^{-15}–10^{-14} m^2 s^{-1}. These diffusivity values are well below those of free-moving molecules in the liquid phase (generally, values lie between 10^{-7} and 10^{-11} m^2 s^{-1}) and are comparable to diffusion rates encountered in typical solid-state reactions. Accessing the thiol sites in the mesopore channels of these adsorbents is therefore an unexpectedly slow process. The diffusivity values, however, increase as a function of increasing thiol group loading in the adsorbents, demonstrating the crucial impact of binding site density on both the binding energetics of the system (Figure 6) and the transfer of ions from the aqueous phase to the binding sites within the adsorbent particles.

The uptake results also show that the diffusivity of the mercury ions is not constant throughout the adsorption process. Surprisingly, the diffusion coefficients *increase* as a function of time (Figure 8a), reaching somewhat constant values upon approaching saturation of the binding sites. When expressed as a function of binding site coverage (θ), the D_p values are found to increase in a seemingly linear fashion until full coverage is achieved (Figure 8b). The accelerating mercury ion diffusivity observed in these materials indicates that the ion uptake process in the microspherical adsorbents is autosynergistic, with the presence of mercury ions within the adsorbent assisting in the increasingly rapid adsorption of additional mercury ions. Moreover, the dependence of the D_p values on coverage becomes more significant as the thiol group loading in the materials increases, as indicated by the increasing slope of the plots shown in Figure 8b.

Mercury Ion Adsorption Process. The near-zero D_p values measured at low ion coverage (Figure 8b) suggest that the mercury ions are initially very reluctant to enter the pore channels. Despite the thermodynamically strong interactions between mercury ions and thiols, the very low initial ion flux appears to impede the accessibility of the thiol groups when these are present within the channels of a mesoporous framework. Judging from this observation, it can be speculated that the previously reported inability of thiol-loaded mesostructures to adsorb metals ions other than Hg^{2+} (viz., Cd^{2+}, Pb^{2+}, Zn^{2+}, Co^{3+}, Fe^{3+}, Cu^{2+}, and Ni^{2+})[30] can, in fact, be ascribed to the prohibitively high diffusion barriers preventing these ions from entering the mesopore channels of the adsorbents.

Figure 9 depicts the possible processes involved in the mercury ion flux inside the channels of a mesostructure pore channel. We propose that the environment of the thiol-loaded pore channels is initially somewhat hydrophobic, resulting in the observed initial slow infiltration of the aqueous-phase ions inside the pore channels. Once complexation occurs, however, the pore environment becomes more hydrophilic (plausibly as a result of the formation of charged $-SHg^{+}$ moieties) up to the adsorption shock front of the pore channel (Figure 9), allowing for the entry of solvated mercury ions inside the pore channels. These uncomplexed ions can then advance the adsorption shock front by eventually binding with the free thiol ligands further down the pore channels. Consistent with the experimentally observed trends, it follows that adsorbents that have high surface densities of thiol groups (i.e., MP-MSU-6%) will favor the probability of advancing the shock front by allowing the rapid transfer of displaced ions to uncomplexed thiol groups in the pore channels (Figure 9), resulting in

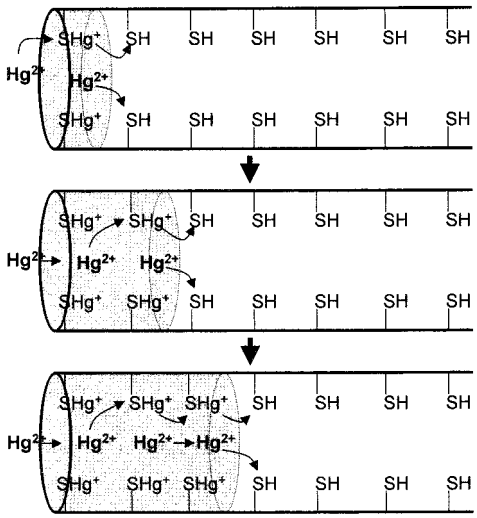

Figure 9. Depiction of the diffusion process of mercury ions inside a MP-MSU mesopore. As the adsorption shock front (shown as a dotted circle) advances, the hydrophilic region of the pore channel (shown as the shaded area) expands, allowing the permeation of free mercury ions from the solution. The displacement of thiol-complexed mercury by free ions becomes increasingly frequent as the adsorption shock front advances.

higher ion fluxes (Figure 8). In contrast, the shock front advancement in adsorbents with highly dispersed thiol groups (such as MP-MSU-2%) will be greatly disadvantaged because of the increased improbability of ions crossing the hydrophobic boundary between the adsorption front and the more distant uncomplexed thiol site.

In addition, the observed accelerating diffusivity of the ions inside the mesostructures (Figure 8) suggests that competitive displacement of the thiol-complexed ions (i.e., the expulsion of a complexed mercury ion from a thiol group by an incoming free mercury ion) might also be occurring inside the adsorbent pores. As the adsorption proceeds, the pore channels become increasingly populated with complexed and free mercury ions. This increases the number of potential mercury ion displacements inside the pore channels, assisting in the propagation of free mercury ions through the pore (Figure 9), and consequently accelerating the overall ion flux in the adsorbents.

The observed slow uptake of the Hg^{2+} ions by the microspheres is exacerbated by the fact that the adsorbent particles are relatively large and devoid of any textural porosity, which means that the ions can only diffuse into the particles from a restricted number of pore channel openings located at the periphery of the microspheres. In contrast, relatively rapid uptake of mercury ions has been reported for thiol-functionalized HMS silica (MP−HMS), with 70% of the thiol sites being bound by mercury ions within 1 min of exposure.[32] Unlike the microspheres used in the present work, MP−HMS exhibits a high degree of textural porosity, thus resulting in improved access to the very large number of pore channel openings that can rapidly be reached by the ions. The rapid ion uptake by MP−HMS can therefore be ascribed to the abundant openings to the mesopore channels that are thus exposed to the solution, effectively offsetting the inherently slow migration of the mercury ions within the pores of the adsorbent.

Conclusion

By studying the mercury ion adsorption characteristics of uniform-sized thiol-functionalized microspherical MSU-X mesostructures devoid of any textural porosity, new insight has been gained into the thermodynamic and kinetic processes involved in the adsorption of these ions within the pore channels of mesostructured adsorbents.

This work has shown that, unlike thiol-functionalized mesostructures composed of submicron-sized particles, which exhibit type-I adsorption isotherms for mercury ion adsorption, the absence of textural porosity in the microspherical mesostructures results in reduced binding affinity for mercury ions at low concentrations.

This research also demonstrated the successful application of the shrinking core model in the determination of mercury ion diffusion coefficients within the microspheres. Surprisingly, the results show that, despite the relatively large and unobstructed pore channels of the adsorbents (and also contrary to anecdotal assumptions), the diffusion of metal ions within the mesopore channels of surfactant-assembled oxides is, in fact, a very slow process, with diffusion coefficients more characteristic of solid-phase reactions than those typically found in fluid systems. Equally surprising is the observed acceleration of the mercury ion diffusion rate as saturation of the binding site is approached.

The results of this work raise important considerations regarding the practical applications of mesoporous adsorbents in flowing systems such as fixed- and fluidized-bed reactors and liquid chromatography. Because these applications often involve very high effluent flow rates, it can be surmised that the majority of the binding sites within mesostructured microspherical adsorbents (and mesostructures devoid of textural porosity) can never be accessed by targeted adsorbate ions because of the slow diffusion kinetics of these materials. On the other hand, mesostructures with high degrees of textural porosity, such as HMS silica, might be less susceptible to this limitation. The results obtained from this research thus emphasizes the impact that particle morphology has on the practical implementation of mesostructured materials in industrially relevant processes.

Acknowledgment. We acknowledge the Natural Sciences and Engineering Research Council of Canada (NSERC) for financial support. We also thank L. Semenyna (Ontario Geosciences Laboratory) for providing technical support with SEM.

CM0112082